Triaxiality and exotic rotations at high spins in ^{134}Ce

C. M. Petrache,[1] S. Guo,[1,*] A. D. Ayangeakaa,[2,†] U. Garg,[2] J. T. Matta,[2,‡] B. K. Nayak,[2,§] D. Patel,[2,‖] M. P. Carpenter,[3] C. J. Chiara,[3,4,¶] R. V. F. Janssens,[3] F. G. Kondev,[5] T. Lauritsen,[3] D. Seweryniak,[3] S. Zhu,[3] S. S. Ghugre,[6] and R. Palit[7,8]

[1]*Centre de Sciences Nucléaires et Sciences de la Matière, CNRS/IN2P3, Université Paris-Saclay, Bâtiment 104-108, 91405 Orsay, France*

[2]*Department of Physics, University of Notre Dame, Notre Dame, Indiana 46556, USA*

[3]*Physics Division, Argonne National Laboratory, Argonne, Illinois 60439, USA*

[4]*Department of Chemistry and Biochemistry, University of Maryland, College Park, Maryland 20742, USA*

[5]*Nuclear Engineering Division, Argonne National Laboratory, Argonne, Illinois 60439, USA*

[6]*UGC-DAE Consortium for Science Research, Kolkata 700 098, India*

[7]*Tata Institute of Fundamental Research, Mumbai 400 005, India*

[8]*The Joint Institute for Nuclear Astrophysics, University of Notre Dame, Notre Dame, Indiana 46556, USA*

(Received 11 April 2016; published 6 June 2016)

High-spin states in ^{134}Ce have been investigated using the ^{116}Cd(^{22}Ne,$4n$) reaction and the Gammasphere array. The level scheme has been extended to an excitation energy of $\sim$30 MeV and spin $\sim$54 $\hbar$. Two new dipole bands and four new sequences of quadrupole transitions were identified. Several new transitions have been added to a number of known bands. One of the strongly populated dipole bands was revised and placed differently in the level scheme, resolving a discrepancy between experiment and model calculations reported previously. Configurations are assigned to the observed bands based on cranked Nilsson-Strutinsky calculations. A coherent understanding of the various excitations, both at low and high spins, is thus obtained, supporting an interpretation in terms of coexistence of stable triaxial, highly deformed, and superdeformed shapes up to very high spins. Rotations around different axes of the triaxial nucleus, and sudden changes of the rotation axis in specific configurations, are identified, further elucidating the nature of high-spin collective excitations in the $A = 130$ mass region.

DOI: 10.1103/PhysRevC.93.064305

I. INTRODUCTION

The structure of the ^{134}Ce nucleus has been studied in detail at low and medium spins using both in-beam [1–5] techniques and β-decay methods [6], leading to detailed knowledge of its low-spin structure. At high spins, on the other hand, the available information is rather sparse. Some time ago, two triaxial and one superdeformed (SD) bands were identified in a measurement using the 8π array [7], and the only other recent results were obtained as a byproduct of a Gammasphere experiment focused on ^{134}Pr [8] wherein the SD band was confirmed and the yrast, positive-parity band was extended by two transitions (one tentative).

The primary interest in studying nuclei in this mass region, and in particular ^{134}Ce, stems from the recent discoveries of multiple chiral partner bands in ^{133}Ce [9], and of transverse wobbling in ^{135}Pr [10]. The chiral and wobbling modes are the only unambiguous experimental indications of nuclear triaxiality thus far. As ^{134}Ce can be considered to be the core of both ^{133}Ce and ^{135}Pr, a detailed investigation of this nucleus could provide further evidence for, and understanding of, the triaxial behavior exhibited by nuclei in this region.

This work is also motivated by the experimental difficulties in obtaining a coherent and conclusive understanding of the dipole bands recently identified in ^{134}Ce [5]. For example, negative parity was assigned to both dipole bands observed in ^{134}Ce, while the corresponding bands in ^{133}Ce, obtained by coupling an $h_{11/2}$ neutron hole to the dipole bands in ^{134}Ce, are assigned both positive and negative parities [9]. In addition, a complete understanding of competition between triaxial and highly deformed or SD configurations in the $A = 130$ mass region has not yet been achieved. Two types of strongly deformed bands have been observed in this region: the highly deformed ones in the Nd nuclei ($\varepsilon_2 \approx 0.3$), which involve only neutron intruders from above the $N = 82$ ($\nu i_{13/2}, \nu f_{7/2}, \nu h_{9/2}$) shell closure, and the SD sequences in the Ce nuclei (with larger deformation, $\varepsilon_2 \approx 0.4$), which involve, in addition to the aforementioned neutron intruders, the proton extruders ($\pi g_{9/2}$) from below the $Z = 50$ gap [11].

A further motivation of this work is to study the evolution of triaxiality in Ce nuclei, with the aim of verifying the extent to which the conclusions drawn from the study of Nd sequences [12–17] are applicable to similar bands of neighboring nuclei. Unfortunately, it has not hitherto been possible to draw any definite conclusions on the structure of the triaxial bands in ^{133,134}Ce [7,18] as none of the observed structures were linked to low-lying states. (Only very recently

*On leave from Institute of Modern Physics, Chinese Academy of Sciences, Lanzhou 730000, China.

†Present address: Physics Division, Argonne National Laboratory, Argonne, Illinois 60439, USA.

‡Present address: Physics Division, Oak Ridge National Laboratory, Oak Ridge, Tennessee 37830, USA.

§Present address: Nuclear Physics Division, Bhabha Atomic Research Center (BARC), Mumbai 400085, India.

‖Present address: M.D. Anderson Cancer Center, Houston, Texas 77030, USA.

¶Present address: US Army Research Laboratory, Adelphi, Maryland 20783, USA.

have the triaxial bands in ^{133}Ce been linked to low-lying levels [19]).

The present paper reports new experimental results, both at low and at high spins, in ^{134}Ce. These were obtained from a high-statistics Gammasphere experiment. Six new bands are identified, one at low spins and five at high angular momenta. One of the two previously reported dipole bands is revised significantly, based on the observation of several new transitions linking it to low-lying states. The observed bands are discussed within the framework of the cranked Nilsson-Strutinsky (CNS) model, as described in Refs. [20–23]. Configurations based on triaxially deformed minima are proposed for nearly all observed bands on the basis of the good agreement between experimental data and results of the CNS calculations. In addition, a new configuration is proposed for the SD band.

II. EXPERIMENTAL DETAILS

The present work is the third in a series of papers reporting results from the same measurement. Thus, the experimental procedure and the analysis methods are similar and only briefly summarized here. The reader is referred to Refs. [9,19] for further details. The experiment was performed at the ATLAS facility at Argonne National Laboratory where high-spin states in ^{134}Ce were populated in two separate experiments following the ^{116}Cd(^{22}Ne, $4n$) reaction. In the first one, a 112-MeV beam of ^{22}Ne, provided by the ATLAS facility, bombarded a 1.48-mg/cm^2-thick target foil of isotopically enriched ^{116}Cd, sandwiched between a 50-μg/cm^2-thick front layer of Al and a 150-μg/cm^2 Au backing. The second experiment used a similar beam and a target of the same enrichment and thickness evaporated onto a 55-μg/cm^2-thick Au foil. The Gammasphere array [24], which comprised 101 (88) active Compton-suppressed high-purity germanium (HPGe) detectors during the first (second) experiment, was used to detect the γ rays emitted by the recoiling nuclei. The accumulated events were unfolded and sorted into fully symmetrized, three-dimensional (E_γ-E_γ-E_γ) and four-dimensional (E_γ-E_γ-E_γ-E_γ) histograms and analyzed using the RADWARE [25,26] analysis package. Spin and parity assignments were made on the basis of an extensive angular-distribution measurement [27] and, for weak transitions, on a two-point angular-correlation (anisotropy) ratio, R_{ac} [28,29].

III. RESULTS AND LEVEL SCHEME

The level scheme of ^{134}Ce obtained in the present work is presented in Figs. 1 and 2. Compared to previous works (cf. Ref. [5]), it is considerably extended and several new dipole and quadrupole sequences have been identified. As mentioned earlier, multipolarities of the newly identified γ-ray transitions were inferred from a combination of angular-distribution and two-point angular-correlation analyses. Transition energies, angular-distribution coefficients and anisotropies, as well as the suggested spins and parities are presented in Table I.

A. The dipole bands

Coincidence spectra obtained by double-gating on selected transitions of the previously reported dipole sequences are provided in Fig. 3, while those from double gates on selected transitions of the newly identified dipole bands are presented in Fig. 4.

Band $D1$ was first reported in Ref. [5]. The present results confirm all the in-band dipole and quadrupole crossover transitions, with the exception of the highest 996-keV one. The connecting transitions to low-lying states reported in Ref. [5] are not observed, however. Instead, 14 new transitions deexciting the sequence towards band 1 (577, 581, and 742 keV), band 2 (703 keV), band 7 (347 and 372 keV), band 8 (1352 keV), band 9 (675, 680, 812, and 841 keV), and toward three non-yrast "floating" states—i.e., those not linked to the low-lying levels (161, 202, and 321 keV)—were identified. The sequence has also been extended to higher spins, by adding two dipole transitions of 498 and 520 keV, and four quadrupole ones of 826, 974, 990, and 1018 keV.

The positive parity assigned to band $D1$ is determined by the $E2$ character of the 703-keV transition linking it to band 1 and by the mixed $M1/E2$ character of the 347-, 372-, and 841-keV γ rays that connect it to the positive-parity bands 7 and 9 (see Table I). This assignment is in contrast to the results of Ref. [5] in which a negative parity was assigned to band $D1$, based on the $E1$ character of the 664-keV transition (not seen in this work). It is surmised that the latter transition was, most likely a contaminant. Indeed, when double-gating on the same 196- and 239-keV γ rays used in producing the spectrum displayed in Fig. 3 of Ref. [5], it is apparent that the 664-keV transition is missing, while the 660- and 667-keV lines from the lower part of the level scheme are present (see Fig. 3). On the other hand, the 664-keV transition is strong and is clearly seen in the spectrum double-gated on the 372- and 239-keV γ rays, fixing the decay of band $D1$ to the 11^+ level of band 7, which then decays to the band 9 via the 665 keV transition. Moreover, the anisotropy ratios of the other decay-out transitions of band $D1$ reported in Ref. [5] have either very large errors [e.g., $R_{ac} = 1.57(94)$ for the 783-keV transition], or are not measured (e.g., the 1030-keV line). Summarizing, the present results on band $D1$ are in disagreement with those of Ref. [5] and definitively fix its excitation energy, spins and positive parity.

Band $D2$ was first reported in Ref. [5]. Double-gated coincidence spectra showing the in-band transitions and the decay towards band 8 are given in Fig. 3. The present results confirm all the in-band and decay-out transitions, with the exception of the highest 548-keV in-band γ ray and the 574- and 947-keV decay-out transitions that were reported in Ref. [5] but have not been observed in the present data. Three dipole transitions of 489, 522, and 666 keV, and three quadrupole crossover ones of 978, 1009, and 1012 keV are newly identified and placed in the higher part of the band. Five new transitions of 477, 639, 736, 956, and 988 keV were added to the decay out of band $D2$. The 956-keV γ ray was previously placed in band 4. The present data indicate instead that this line is a connecting transition between bands $D2$ and band 4, which continues to higher spins, with two new $E2$

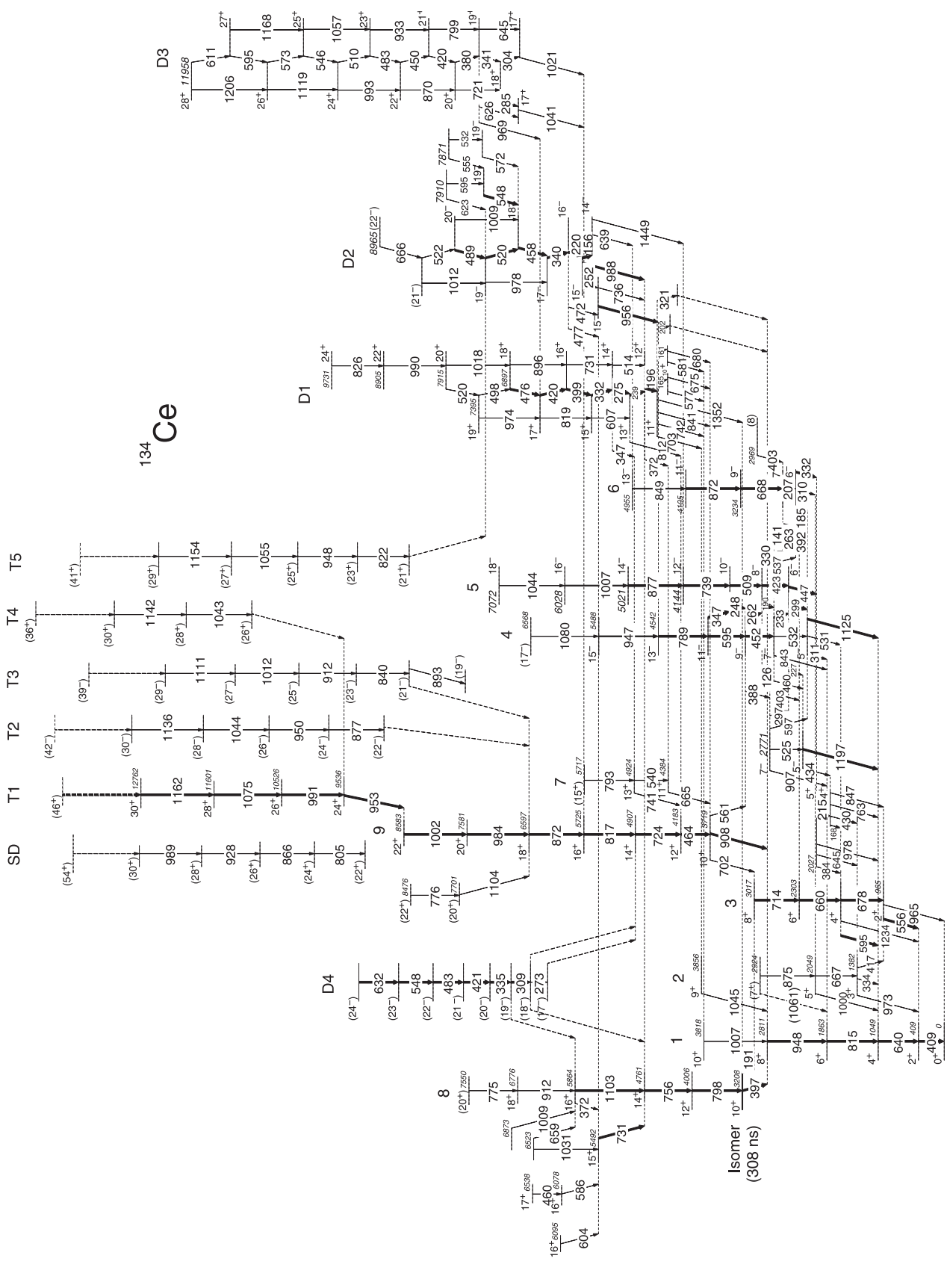

FIG. 1. Partial level scheme of ^{134}Ce obtained in the present work. Arrow widths represent the intensities of the γ rays. The half-life of the 10^+ level in band 8 is taken from Ref. [30]. Continuation of the high-spin part is presented in Fig. 2.

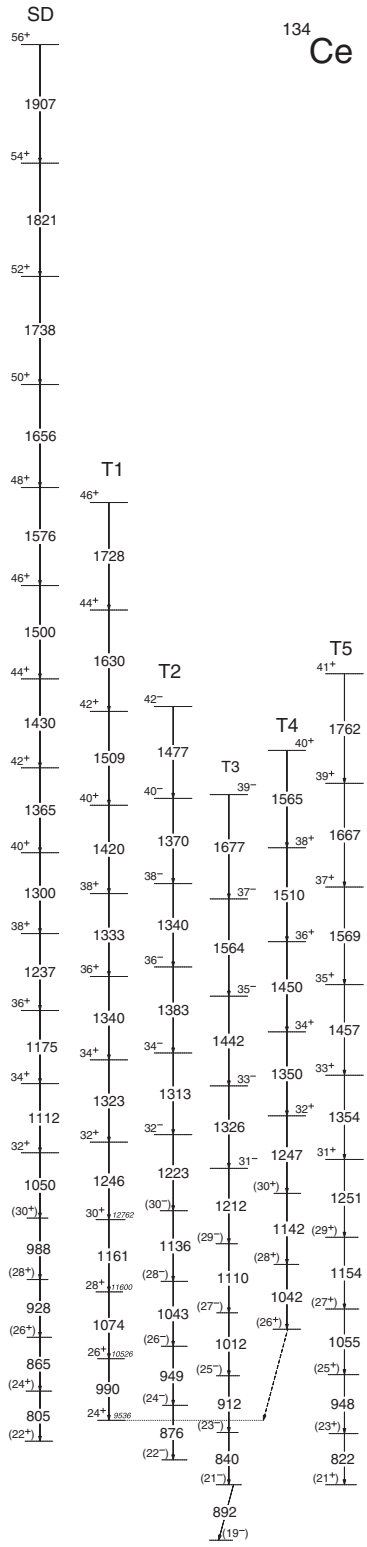

FIG. 2. Partial level scheme of ^{134}Ce showing the continuation of the high-spin bands of Fig. 1.

transitions of 947 and 1080 keV. Two new parallel cascades feeding the 18^- and 19^- states of band $D2$ are also identified. The parity of the band is fixed by the 956- and 1449-keV $E2$ transitions (see Table I) and the polarization measurements reported in Ref. [5].

Bands $D3$ and $D4$ have been observed for the first time in the present work. Band $D3$ consists of 12 levels connected by dipole and quadrupole crossover transitions. A sum of coincidence spectra double gated on the in-band transitions is provided in Fig. 4. This sequence is linked to the 16^+ level of band 9 directly through the 1021-keV $M1/E2$ transition, and indirectly through an intermediate 6765-keV, 17^+ state populated by the 285- and 626-keV transitions and deexcited by the 1041-keV $M1/E2\,\gamma$ ray. The parity of the band is positive, being fixed by the 1021-keV $M1/E2$ transition to the 16^+ state of the yrast band 9.

Band $D4$ consists of eight levels connected by dipole transitions. A sum of coincidence spectra double gated on the in-band γ rays is provided in Fig. 4. The decay out of this band could not be conclusively established, although there are clear indications that it feeds the 14^+ and 16^+ levels of band 8, as well as the 14^+ state of band 9. The excitation energies, spins and parity are, therefore, undetermined. The suggested spin-parity assignments of the states, based on the theoretical interpretation discussed in Sec. IV, are indicated in parentheses in Fig. 1 and Table I.

B. The quadrupole bands

Four new sequences of quadrupole transitions have been identified based on this work: two at low and medium spins (bands 6 and 7), and two at high angular momenta ($T4$ and $T5$). Spectra obtained by doubly-gating on selected transitions in band 8 are presented in Fig. 5, while spectra for the high-spin triaxial and SD bands are found in Figs. 6 and 7. For the low- and medium-spin sequences, two transitions are added at the top of band 4 (947 and 1080 keV), one at the top of band 5 (1044 keV), and thirteen to the lower parts of bands 4 and 5 (126, 141, 227, 299, 311, 403, 434, 460, 525, 531, 597, 907, and 1197 keV).

The bands labeled 6 and 7 in Fig. 1 have been observed here for the first time. Band 6 consists of four levels and decays primarily through the 207-keV γ ray to the 6^- state at 2359 keV and through the 263- and 392-keV lines to bands 3 and 4, respectively. Band 7, on the other hand, consists of three states and decays to band 9 via the 665- and 741-keV transitions of mixed $M1/E2$ character.

The sequence labeled as band 8 was first reported in Ref. [2] and is built on the 10^+ isomer whose lifetime was measured to be $T_{1/2} = 336(14)$ ns in Ref. [2] and $T_{1/2} = 308(5)$ ns in Ref. [30]. The 731-keV transition reported in Refs. [2,3] is confirmed and is found to be of $M1/E2$ character, leading to a 15^+ state at 5492 keV. Four new γ rays of 460, 586, 604, and 1031 keV are placed above this level. The tentative 1103-keV transition reported in Ref. [2] is confirmed and is determined to be of $E2$ character. Four new lines of 659, 775, 912, and 1009 keV are placed above this level.

Band 9 extends up to spin 22^+ where a crossing with band $T1$ is observed. The latter band was observed up to spin (38^+) in Ref. [8]. The present data confirm all the transitions, with the exception of the highest, 1350-keV tentative γ ray reported therein. Instead, five new transitions of 1333, 1420,

TABLE I. Energies of γ rays, initial level energies, angular-distribution coefficients (A_2, A_4), anisotropy ratios (R_{ac}), multipolarities, and spin-parity assignments for the associated states in ^{134}Ce. The transitions are grouped in bands and the transitions connecting a given band to low-lying states are listed at the end of each band.

γ energy [a]	E_i (keV)	A_2	A_4	R_{ac}	Multipolarity[b]	$I_i^\pi \rightarrow I_f^\pi$
Band 1						
409.1	409.1				$E2^{M,L}$	$2^+ \rightarrow 0^+$
639.7	1048.8				$E2^{M}$	$4^+ \rightarrow 2^+$
814.5	1863.3				$E2^{M}$	$6^+ \rightarrow 4^+$
947.8	2811.1				$E2^{M}$	$8^+ \rightarrow 6^+$
1006.5	3817.6				$E2^{M}$	$10^+ \rightarrow 8^+$
Band 2						
666.7	2049.0				$E2^{M}$	$5^+ \rightarrow 3^+$
875.4	2924.4					$7^+ \rightarrow 5^+$
333.5	1382.3					$3^+ \rightarrow 4^+$
417.4	1382.3				$M1/E2^{M,G}$	$3^+ \rightarrow 2^+$
973.2	1382.3				$M1/E2^{M,G}$	$3^+ \rightarrow 2^+$
1000.2	2049.0				$M1/E2^{G}$	$5^+ \rightarrow 4^+$
1045.2	3856.3	−0.42(4)	0.08(5)	0.73(5)	$M1/E2$	$9^+ \rightarrow 8^+$
(1061.1)	2924.4					$7^+ \rightarrow 6^+$
Band 3						
659.9	2303.3				$E2^{M}$	$6^+ \rightarrow 4^+$
678.5	1643.4				$E2^{M}$	$4^+ \rightarrow 2^+$
713.9	3017.2				$E2^{M}$	$8^+ \rightarrow 6^+$
555.8	964.9				$M1/E2^{M,G}$	$2^+ \rightarrow 2^+$
594.6	1643.4				$M1/E2^{M,G}$	$4^+ \rightarrow 4^+$
964.9	964.9				$E2^{M}$	$2^+ \rightarrow 0^+$
1234.3	1643.4				$E2^{M}$	$4^+ \rightarrow 2^+$
Low-spin states						
168.4	1811.8				$M1/E2^{G}$	$4^+ \rightarrow 4^+$
215.1	2026.9				$M1/E2^{M}$	$5^+ \rightarrow 4^+$
297.1	2770.5					$7^- \rightarrow 6^-$
383.5	2026.9				$M1/E2^{M}$	$5^+ \rightarrow 4^+$
429.5	1811.8				$M1/E2^{M}$	$4^+ \rightarrow 3^+$
434.2	2246.0					$5^- \rightarrow 4^+$
524.5	2770.5					$7^- \rightarrow 5^-$
596.5	2770.5					$7^- \rightarrow 5^-$
644.6	2026.9				$E2^{M}$	$5^+ \rightarrow 3^+$
763.0	1811.8				$M1/E2^{M}$	$4^+ \rightarrow 4^+$
847.3	1811.8				$E2^{M}$	$4^+ \rightarrow 2^+$
907.2	2770.5					$7^- \rightarrow 6^+$
978.1	2026.9				$M1/E2^{M,G}$	$5^+ \rightarrow 4^+$
1197.2	2246.0	−0.14(5)	0.03(7)	0.91(8)	$E1$	$5^- \rightarrow 4^+$
Band 4						
532.1	2706.1				$E2^{M,L}$	$7^- \rightarrow 5^-$
451.9	3158.0				$E2^{M,L}$	$9^- \rightarrow 7^-$
594.5	3752.5				$E2^{L}$	$11^- \rightarrow 9^-$
789.1	4541.6				$E2^{L}$	$13^- \rightarrow 11^-$
946.5	5488.1	0.35(4)	−0.15(5)	1.37(9)	$E2$	$15^- \rightarrow 13^-$
1079.5	6567.6					$(17^-) \rightarrow 15^-$
140.8	2706.1					$7^- \rightarrow 7^-$
232.7	2706.1				$M1/E2^{M}$	$7^- \rightarrow 6^-$
262.0	3158.0	−0.23(8)	0.08(11)	0.80(7)	$M1/E2$	$9^- \rightarrow 8^-$
310.7	2174.0					$5^- \rightarrow 6^+$
346.9	3752.5					$11^- \rightarrow 10^-$
387.5	3158.0					$9^- \rightarrow 7^-$
402.8	2706.1					$7^- \rightarrow 6^+$
460.1	2706.1					$7^- \rightarrow 5^-$
530.6	2174.0	−0.09(1)	−0.01(2)	0.95(7)	$E1$	$5^- \rightarrow 4^+$

TABLE I. (*Continued.*)

γ energy [a]	E_i (keV)	A_2	A_4	R_{ac}	Multipolarity[b]	$I_i^\pi \rightarrow I_f^\pi$
842.8	2706.1					$7^- \rightarrow 6^+$
1125.2	2174.0	−0.18(3)	0.05(4)	0.83(5)	$E1$	$5^- \rightarrow 4^+$
Band 5						
422.6	2896.0				$E2^{M,L}$	$8^- \rightarrow 6^-$
509.2	3405.6				$E2^{M,L}$	$10^- \rightarrow 8^-$
738.5	4144.1				$E2^{M,L}$	$12^- \rightarrow 10^-$
877.2	5021.3				$E2^{L}$	$14^- \rightarrow 12^-$
1006.5	6027.8				$E2^{L}$	$16^- \rightarrow 14^-$
1044.3	7072.1				$E2^{L}$	$18^- \rightarrow 16^-$
125.5	2896.0					$8^- \rightarrow 7^-$
189.9	2896.0				$M1/E2^{M}$	$8^- \rightarrow 7^-$
227.4	2473.4					$6^- \rightarrow 5^-$
247.6	3405.6					$10^- \rightarrow 9^-$
299.4	2473.4				$M1/E2^{M}$	$6^- \rightarrow 5^-$
330.3	2896.0					$8^- \rightarrow 7^-$
446.5	2473.4				$E1^{M}$	$6^- \rightarrow 5^+$
537.4	2896.0				$E2^{M}$	$8^- \rightarrow 6^-$
Band 6						
667.8	3233.5	0.36(5)	−0.03(6)	1.34(9)	$E2$	$9^- \rightarrow 7^-$
871.8	4105.3	0.31(2)	−0.17(2)	1.20(10)	$E2$	$11^- \rightarrow 9^-$
849.2	4954.5	0.17(4)	−0.14(6)	1.19(10)	$E2$	$13^- \rightarrow 11^-$
184.6	2358.6				$M1/E2^{M}$	$6^- \rightarrow 5^-$
207.1	2565.7	−0.44(3)	0.08(5)	0.69(5)	$M1/E2$	$7^- \rightarrow 6^-$
262.5	2565.7				$E1^{M}$	$7^- \rightarrow 6^+$
309.6	2358.6				$E1^{M}$	$6^- \rightarrow 5^+$
331.7	2358.6				$E1^{M}$	$6^- \rightarrow 5^+$
391.7	2565.7				$E2^{M}$	$7^- \rightarrow 5^-$
403.7	2969.4					$(8) \rightarrow 7^-$
Band 7						
540.2	4923.9					$13^+ \rightarrow 11^+$
793.0	5716.9					$(15^+) \rightarrow 13^+$
664.8	4383.7	−0.87(14)	0.19(18)	0.34(4)	$M1/E2$ [$\delta = -2.13(48)$]	$11^+ \rightarrow 10^+$
740.9	4923.9	−0.76(3)	0.18(4)	0.50(6)	$M1/E2$ [$\delta = -1.73(52)$]	$13^+ \rightarrow 12^+$
Band 8						
797.7	4005.6	0.36(3)	−0.02(4)	1.31(8)	$E2$	$12^+ \rightarrow 10^+$
755.8	4761.4	0.13(2)	−0.12(8)	1.09(7)	$E2$	$14^+ \rightarrow 12^+$
1102.5	5863.9	0.24(3)	−0.06(4)	1.22(8)	$E2$	$16^+ \rightarrow 14^+$
911.6	6775.5	0.42(7)	−0.08(9)	1.38(9)	$E2$	$18^+ \rightarrow 16^+$
774.7	7550.2					$(20^+) \rightarrow 18^+$
730.5	5491.9	−0.23(2)	0.04(2)	0.82(5)	$M1/E2$	$15^+ \rightarrow 14^+$
586.2	6078.1	−0.14(4)	0.14(5)	0.83(6)	$M1/E2$	$16^+ \rightarrow 15^+$
460.0	6538.1	−0.33(2)	0.03(3)	0.76(7)	$M1/E2$	$17^+ \rightarrow 16^+$
603.5	6095.4	−0.55(9)	0.61(13)	0.56(6)	$M1/E2$	$16^+ \rightarrow 15^+$
659.0	6522.9					$\rightarrow 16^+$
1031.0	6522.9					$\rightarrow 15^+$
1009.0	6872.9					$\rightarrow 16^+$
372.0	5863.9					$16^+ \rightarrow 15^+$
191.2	3207.9				$E2^{M}$	$10^+ \rightarrow 8^+$
396.8	3207.9				$E2^{M}$	$10^+ \rightarrow 8^+$
Band 9						
464.1	4183.0					$12^+ \rightarrow 10^+$
724.3	4907.3					$14^+ \rightarrow 12^+$
817.2	5724.5					$16^+ \rightarrow 14^+$
872.1	6596.6					$18^+ \rightarrow 16^+$
984.1	7580.7	0.41(2)	−0.11(3)	1.46(10)	$E2$	$20^+ \rightarrow 18^+$
1002.2	8582.9	0.51(8)	−0.13(11)	1.61(12)	$E2$	$22^+ \rightarrow 20^+$

TABLE I. (*Continued.*)

γ energy [a]	E_i (keV)	A_2	A_4	R_{ac}	Multipolarity[b]	$I_i^\pi \rightarrow I_f^\pi$
560.9	3718.9					$10^+ \rightarrow 9^-$
701.7	3718.9				$E2^M$	$10^+ \rightarrow 8^+$
775.6	8476.3					
907.8	3718.9				$E2^M$	$10^+ \rightarrow 8^+$
1104.1	7700.7					
Band*D*1						
165.4	4559.6				$M1/E2^L$	$11^+ \rightarrow 10^+$
196.4	4756.0				$M1/E2^L$	$12^+ \rightarrow 11^+$
239.0	4995.0				$M1/E2^L$	$13^+ \rightarrow 12^+$
275.4	5270.4				$M1/E2^L$	$14^+ \rightarrow 13^+$
331.9	5602.3				$M1/E2^L$	$15^+ \rightarrow 14^+$
399.1	6001.4				$M1/E2^L$	$16^+ \rightarrow 15^+$
420.1	6421.5				$M1/E2^L$	$17^+ \rightarrow 16^+$
475.8	6897.3				$M1/E2^L$	$18^+ \rightarrow 17^+$
498.0	7395.3	−0.53(7)	0.19(9)	0.60(4)	$M1/E2$	$19^+ \rightarrow 18^+$
514.0	5270.4				$E2$	$14^+ \rightarrow 12^+$
519.9	7915.2					$20^+ \rightarrow 19^+$
607.3	5602.3					$15^+ \rightarrow 13^+$
731.0	6001.4					$16^+ \rightarrow 14^+$
819.2	6421.5					$17^+ \rightarrow 15^+$
826.1	9731.4	0.63(6)	−0.51(17)	1.98(45)	$E2$	$24^+ \rightarrow 22^+$
895.9	6897.3					$18^+ \rightarrow 16^+$
973.8	7395.3					$19^+ \rightarrow 17^+$
990.1	8905.3	0.69(11)	0.23(14)	1.60(16)	$E2$	$22^+ \rightarrow 20^+$
1017.9	7915.2	0.38(19)	−0.10(25)	1.18(10)	$E2$	$20^+ \rightarrow 18^+$
161.0	4559.6					$11^+ \rightarrow$
201.9	4559.6					$11^+ \rightarrow$
320.9	4559.6					$11^+ \rightarrow$
346.5	5270.4	−0.76(4)	0.24(5)	0.49(4)	$M1/E2$ [$\delta = -2.05(48)$]	$14^+ \rightarrow 13^+$
372.3	4756.0	−0.72(3)	0.16(4)	0.52(4)	$M1/E2$ [$\delta = -2.23(53)$]	$12^+ \rightarrow 11^+$
576.6	4394.2					$\rightarrow 10^+$
581.0	4398.6					$\rightarrow 10^+$
675.3	4394.2					$\rightarrow 10^+$
679.7	4398.6					$\rightarrow 10^+$
703.4	4559.6	0.22(5)	0.05(6)	1.12(8)	$E2$	$11^+ \rightarrow 9^+$
742.0	4559.6					$11^+ \rightarrow 10^+$
812.0	4995.0					$13^+ \rightarrow 12^+$
840.7	4559.6	−0.92(21)	0.32(27)	0.34(4)	$M1/E2$	$11^+ \rightarrow 10^+$
1351.7	4559.6					$11^+ \rightarrow 10^+$
Band*D*2						
155.6	5749.1				$M1/E2^L$	$15^- \rightarrow 14^-$
219.8	5968.9				$M1/E2^L$	$16^- \rightarrow 15^-$
340.3	6309.2				$M1/E2^L$	$17^- \rightarrow 16^-$
457.6	6766.8				$M1/E2^L$	$18^- \rightarrow 17^-$
489.4	7776.1	−0.27(2)	0.05(3)	0.78(5)	$M1/E2$	$20^- \rightarrow 19^-$
519.9	7286.7				$M1/E2^L$	$19^- \rightarrow 18^-$
522.2	8298.3					$(21^-) \rightarrow 20^-$
532.2	7870.6					$\rightarrow 19^-$
548.4	7315.2	−0.58(5)	0.04(7)	0.59(5)	$M1/E2$	$19^- \rightarrow 18^-$
555.4	7870.6					$\rightarrow 19^-$
571.6	7338.4	−0.17(5)	0.03(6)	0.86(6)	$M1/E2$	$19^- \rightarrow 18^-$
594.9	7910.1					$\rightarrow 19^-$
623.4	7910.1					$\rightarrow 19^-$
666.2	8964.5					$(22^-) \rightarrow (21^-)$
977.5	7286.7					$19^- \rightarrow 17^-$
1009.3	7776.1					$20^- \rightarrow 18^-$
1011.6	8298.3					$(21^-) \rightarrow 19^-$

TABLE I. (*Continued.*)

γ energy [a]	E_i (keV)	A_2	A_4	R_{ac}	Multipolarity[b]	$I_i^\pi \rightarrow I_f^\pi$
251.8	5749.1	0.27(4)	0.17(5)	1.13(10)	$E2$	$15^- \rightarrow 15^-$
471.6	5968.9	−0.65(5)	0.20(7)	0.56(4)	$M1/E2$ [$\delta = -2.52(25)$]	$16^- \rightarrow 15^-$
477.0	5968.9					$16^- \rightarrow 15^+$
639.0	5593.5					$14^- \rightarrow 13^-$
735.9	5497.3					$15^- \rightarrow 14^+$
955.7	5497.3	0.43(8)	0.06(11)	1.33(11)	$E2$	$15^- \rightarrow 13^-$
987.7	5749.1					$15^- \rightarrow 14^+$
1449.4	5593.5	0.56(10)	0.05(13)	1.55(50)	$E2$	$14^- \rightarrow 12^-$
Band*D*3						
304.0	7049.6	−0.31(5)	0.06(7)	0.80(6)	$M1/E2$	$18^+ \rightarrow 17^+$
341.1	7390.7	−0.67(6)	0.23(8)	0.56(4)	$M1/E2$	$19^+ \rightarrow 18^+$
379.8	7770.5	−0.69(8)	0.14(11)	0.59(5)	$M1/E2$	$20^+ \rightarrow 19^+$
419.5	8190.0	−0.70(6)	0.08(8)	0.56(5)	$M1/E2$	$21^+ \rightarrow 20^+$
450.1	8640.1					$22^+ \rightarrow 21^+$
482.7	9122.8					$23^+ \rightarrow 22^+$
510.4	9633.2					$24^+ \rightarrow 23^+$
546.2	10179.4					$25^+ \rightarrow 24^+$
573.0	10752.4					$26^+ \rightarrow 25^+$
594.6	11347.0					$27^+ \rightarrow 26^+$
611.4	11958.4					$28^+ \rightarrow 27^+$
645.1	7390.7					$19^+ \rightarrow 17^+$
720.9	7770.5					$20^+ \rightarrow 18^+$
799.3	8190.0					$21^+ \rightarrow 19^+$
869.6	8640.1	0.25(5)	−0.05(7)	1.21(7)	$E2$	$22^+ \rightarrow 20^+$
932.8	9122.8					$23^+ \rightarrow 21^+$
993.1	9633.2					$24^+ \rightarrow 22^+$
1056.6	10179.4					$25^+ \rightarrow 23^+$
1119.2	10752.4					$26^+ \rightarrow 24^+$
1167.6	11347.0					$27^+ \rightarrow 25^+$
1206.0	11958.4					$28^+ \rightarrow 26^+$
284.6	7049.6					$18^+ \rightarrow 17^+$
625.7	7390.7					$19^+ \rightarrow 17^+$
969.2	7390.7					$19^+ \rightarrow 17^+$
1021.1	6745.6	−0.34(7)	0.20(9)	0.73(6)	$M1/E2$	$17^+ \rightarrow 16^+$
1040.5	6765.0	−0.40(9)	0.26(12)	0.63(5)	$M1/E2$	$17^+ \rightarrow 16^+$
Band*D*4						
272.6						$(18^-) \rightarrow (17^-)$
309.2		−0.36(3)	0.11(4)	0.73(8)	$M1/E2$	$(19^-) \rightarrow (18^-)$
334.5		−0.61(6)	−0.13(8)	0.67(5)	$M1/E2$	$(20^-) \rightarrow (19^-)$
421.2		−0.90(5)	0.20(7)	0.45(3)	$M1/E2$	$(21^-) \rightarrow (20^-)$
482.5		−0.80(8)	−0.03(10)	0.53(6)	$M1/E2$	$(22^-) \rightarrow (21^-)$
547.8		−0.16(9)	0.05(12)	0.80(6)	$M1/E2$	$(23^-) \rightarrow (22^-)$
631.8						$(24^-) \rightarrow (23^-)$
Band*T*1						
990.5	10526.0	0.48(3)	0.03(4)	1.42(11)	$E2$	$26^+ \rightarrow 24^+$
1074.5	11600.5	0.46(3)	−0.05(4)	1.51(10)	$E2$	$28^+ \rightarrow 26^+$
1161.5	12762.0	0.27(9)	−0.02(12)	1.21(21)	$E2$	$30^+ \rightarrow 28^+$
1245.5	14007.5	0.42(8)	0.12(10)	1.25(9)	$E2$	$32^+ \rightarrow 30^+$
1323.0	15330.5					$34^+ \rightarrow 32^+$
1339.5	16670.0					$36^+ \rightarrow 34^+$
1332.5	18002.5					$38^+ \rightarrow 36^+$
1419.5	19422.0					$40^+ \rightarrow 38^+$
1508.5	20930.5					$42^+ \rightarrow 40^+$
1630.0	22560.5					$44^+ \rightarrow 42^+$
1727.5	24288.0					$46^+ \rightarrow 44^+$
953.3	9535.5	0.60(5)	0.04(7)	1.59(15)	$E2$	$24^+ \rightarrow 22^+$

TABLE I. (*Continued.*)

γ energy [a]	E_i (keV)	A_2	A_4	R_{ac}	Multipolarity[b]	$I_i^\pi \rightarrow I_f^\pi$
Band*T*2						
876.5						$(24^-) \rightarrow (22^-)$
949.5		0.35(4)	−0.19(5)	1.36(11)	*E*2	$(26^-) \rightarrow (24^-)$
1043.5		0.26(8)	−0.07(10)	1.16(10)	*E*2	$(28^-) \rightarrow (26^-)$
1136.0		0.38(3)	0.03(3)	1.36(13)	*E*2	$(30^-) \rightarrow (28^-)$
1222.5		0.13(3)	−0.04(4)	1.10(10)	*E*2	$(32^-) \rightarrow (30^-)$
1312.5						$(34^-) \rightarrow (32^-)$
1339.5						$(38^-) \rightarrow (36^-)$
1369.5						$(40^-) \rightarrow (38^-)$
1383.0						$(36^-) \rightarrow (34^-)$
1476.5						$(42^-) \rightarrow (40^-)$
1522						$(44^-) \rightarrow (42^-)$
1606						$(46^-) \rightarrow (44^-)$
Band*T*3						
840.0		0.50(12)	−0.06(16)	1.42(12)	*E*2	$(23^-) \rightarrow (21^-)$
912.0		0.42(8)	0.06(11)	1.31(10)	*E*2	$(25^-) \rightarrow (23^-)$
1012.0		0.32(7)	−0.10(9)	1.27(10)	*E*2	$(27^-) \rightarrow (25^-)$
1110.5		0.34(5)	−0.12(6)	1.39(9)	*E*2	$(29^-) \rightarrow (27^-)$
1212.0						$(31^-) \rightarrow (29^-)$
1326.0						$(33^-) \rightarrow (31^-)$
1442.0						$(35^-) \rightarrow (33^-)$
1563.5						$(37^-) \rightarrow (35^-)$
1677.0						$(39^-) \rightarrow (37^-)$
892.5						$(21^-) \rightarrow (19^-)$
Band*T*4						
1042.5						$(28^+) \rightarrow (26^+)$
1142.0						$(30^+) \rightarrow (28^+)$
1247.0						$(32^+) \rightarrow (30^+)$
1349.5						$(34^+) \rightarrow (32^+)$
1449.5						$(36^+) \rightarrow (34^+)$
1510						$(38^+) \rightarrow (36^+)$
1565						$(40^+) \rightarrow (38^+)$
Band*T*5						
822.0						$(23^+) \rightarrow (21^+)$
948.0						$(25^+) \rightarrow (23^+)$
1055.0						$(27^+) \rightarrow (25^+)$
1153.5						$(29^+) \rightarrow (27^+)$
1250.5						$(31^+) \rightarrow (29^+)$
1353.5						$(33^+) \rightarrow (31^+)$
1457.0						$(35^+) \rightarrow (33^+)$
1568.5						$(37^+) \rightarrow (35^+)$
1667						$(39^+) \rightarrow (37^+)$
1762						$(41^+) \rightarrow (39^+)$
Band SD						
805.0						$(24^+) \rightarrow (22^+)$
865.5						$(26^+) \rightarrow (24^+)$
928.0						$(28^+) \rightarrow (26^+)$
988.5						$(30^+) \rightarrow (28^+)$
1050.0						$(32^+) \rightarrow (30^+)$
1112.0						$(34^+) \rightarrow (32^+)$

TABLE I. (*Continued.*)

γ energy [a]	E_i (keV)	A_2	A_4	R_{ac}	Multipolarity[b]	$I_i^\pi \rightarrow I_f^\pi$
1174.5						$(36^+) \rightarrow (34^+)$
1237.0						$(38^+) \rightarrow (36^+)$
1300.0						$(40^+) \rightarrow (38^+)$
1365.0						$(42^+) \rightarrow (40^+)$
1430.0						$(44^+) \rightarrow (42^+)$
1499.5						$(46^+) \rightarrow (44^+)$
1575.5						$(48^+) \rightarrow (46^+)$
1655.5						$(50^+) \rightarrow (48^+)$
1738.0						$(52^+) \rightarrow (50^+)$
1821						$(54^+) \rightarrow (52^+)$
1907						$(56^+) \rightarrow (54^+)$

[a]The error on the transition energies is 0.2 keV for transitions below 1000 keV and intensities larger than 5% of the ^{134}Ce reaction channel, 0.5 keV for transitions above 1000 keV and intensities lower than 5%, and 1 keV for transitions above 1200 keV and/or weaker than 1%.
[b]The multipolarities of transitions assigned in previous works are indicated as superscripts: "*L*" for Ref. [5], "*M*" for Ref. [3], and "*G*" for Ref. [6].

1509, 1630, and 1728 keV have been identified and added as prolonging the cascade on top of band $T1$.

Bands $T2$, $T3$, and SD were previously reported in Ref. [7]. Band $T2$ is extended to higher spins by three transitions of 1340, 1370, and 1477 keV, and at low spin by the 877-keV line. Band $T3$ is extended to higher spins by three new γ rays of 1442, 1564, and 1677 keV, and at low spins by the 840- and 893-keV transitions. Six new lines are added to the SD band: the 805- and 866-keV transitions at the bottom of the sequence and the 1656-, 1738-, 1821-, and 1907-keV transitions at the top.

Bands $T4$ and $T5$ are new and decay mainly towards bands $T1$ and $D2$, respectively. The decay-out transitions of the two bands could not be established; therefore, their energies, spins, and parity remain uncertain.

IV. DISCUSSION

The level structure of ^{134}Ce, with 58 protons and 76 neutrons, can be considered to arise from an interaction between eight valence proton particles above the $Z = 50$ major shell, and six neutron holes in the $N = 82$ major shell. In the

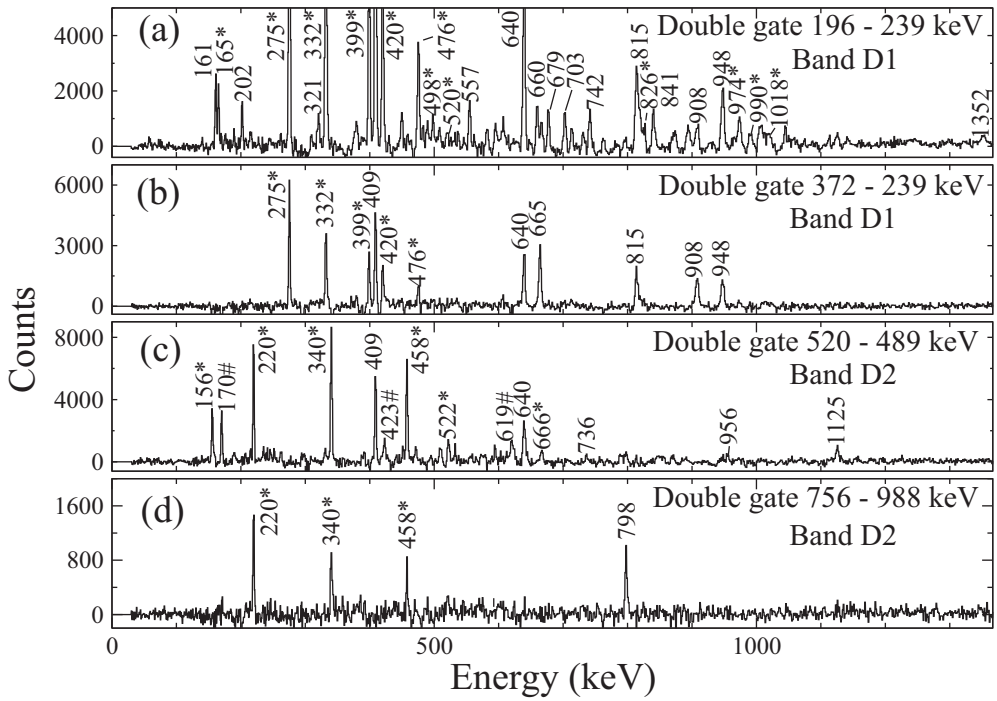

FIG. 3. Double-gated coincidence spectra for bands $D1$ and $D2$ in ^{134}Ce. The gates were set on selected transitions in each band. The transitions marked with # are contaminants from ^{133}Ce, while those marked with an asterisk denote in-band γ rays.

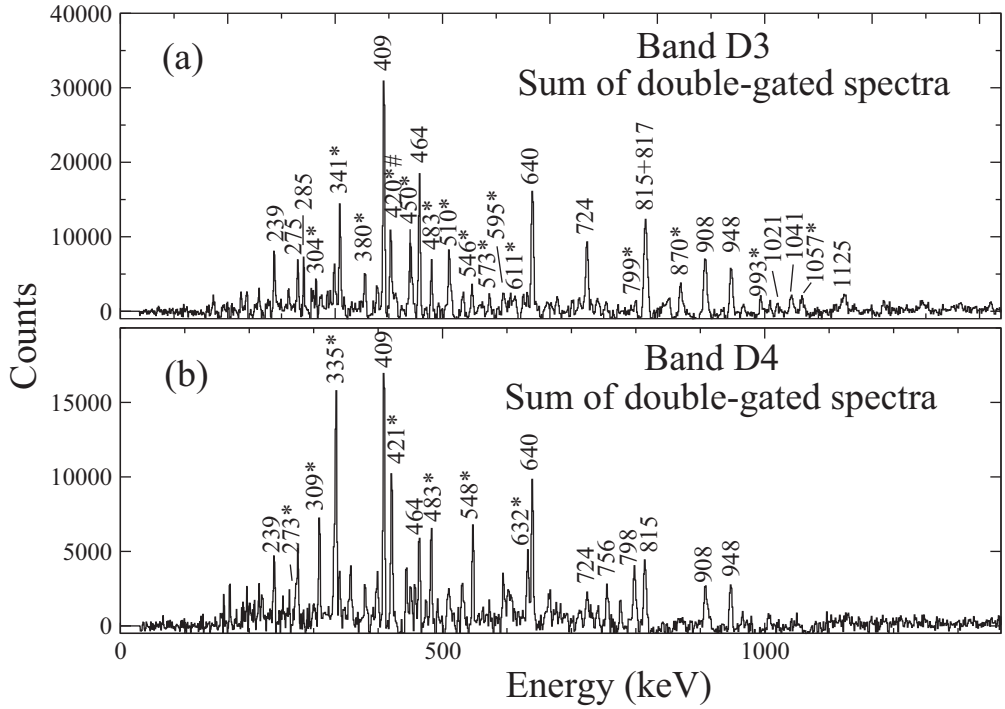

FIG. 4. Sum of spectra double-gated on the in-band dipole transitions for bands $D3$ and $D4$ in ^{134}Ce. The gates were placed on selected transitions of each band. The band transitions are indicated by an asterisk. Contaminants from ^{133}Ce are marked with #.

low-energy regime, the nucleus is expected to be characterized by a small deformation, $\varepsilon_2 \sim 0.15$–0.20. It is appropriate, therefore, to express the single-particle configurations in terms of j-shell quantum numbers.

The configuration assignments proposed for the band structures observed in this work rest on results of calculations performed within the framework of the cranked Nilsson-Strutinsky (CNS) model. In the CNS formalism, the nucleus

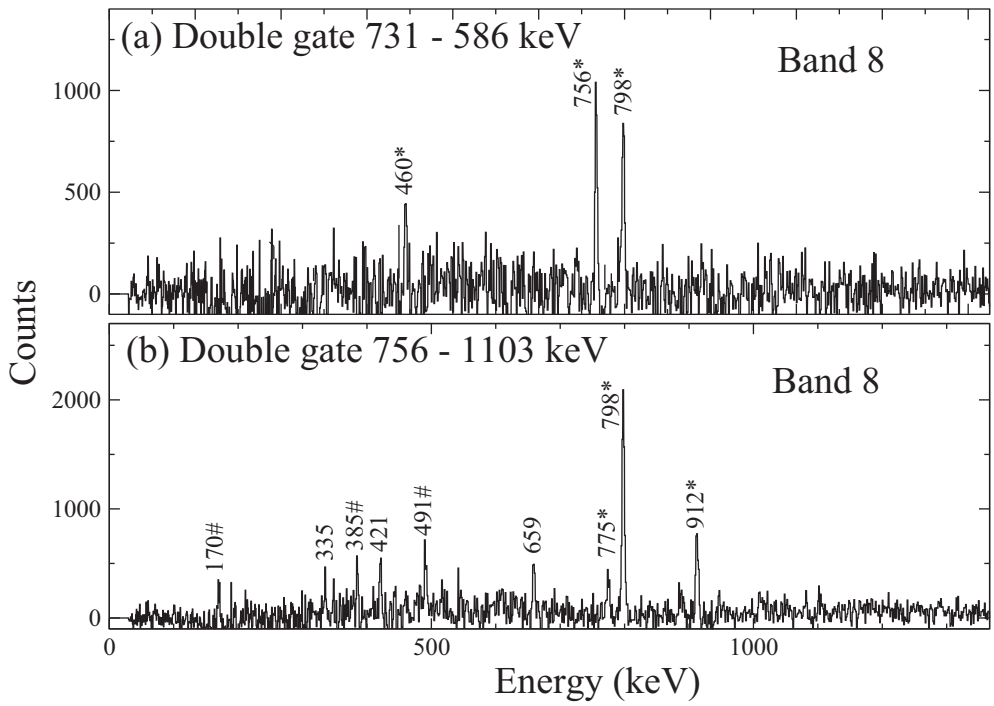

FIG. 5. Double-gated spectra for band 8 of ^{134}Ce. In-band transitions are marked with asterisks, while those marked with # are contaminants from ^{133}Ce.

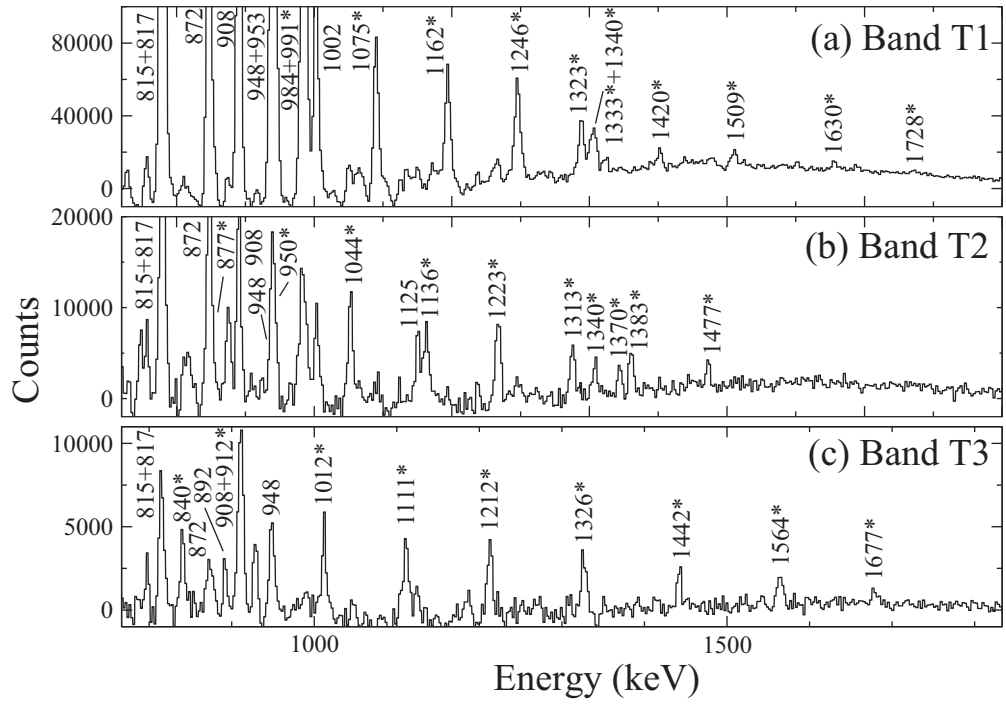

FIG. 6. Double-gated spectra for bands $T1, T2$, and $T3$ of ^{134}Ce. The gates were set on selected transitions in each band: The spectrum of band $T1$ is obtained as the sum of all spectra double gated on the transitions from 953 to 1509 keV. The $T2$ spectrum is the sum of spectra double gated on the transitions from 877 to 1477 keV. The spectrum of band $T3$ is the sum of spectra double gated on the transitions from 840 to 1677 keV. The γ rays marked with asterisks represent the members of the band.

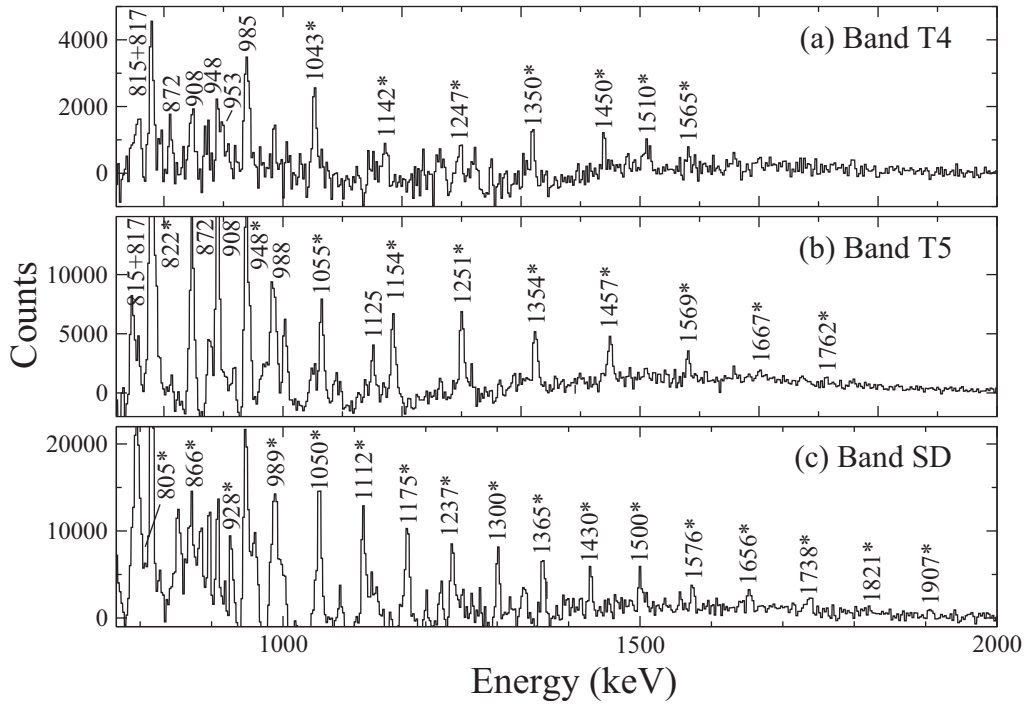

FIG. 7. Double-gated spectra for the $T4$, $T5$, and SD sequences of ^{134}Ce. The gates were set on selected transitions in each band: The spectrum of band $T4$ is the sum of spectra double gated on the transitions from 1043 to 1510 keV. That of band $T5$ is obtained similarly by summing double gates on the in-band transitions, from 822 to 1569 keV, except the 948-keV transition that forms a doublet with the 948-keV γ ray of band 1. The spectrum of band SD results from the sum of double gates on the transitions from 928 to 1576 keV. The transitions marked with asterisks represent the members of the various bands.

rotates about one of its principal axes and pairing is often neglected. The deformation is optimized for each single-particle configuration under consideration. The configurations are labeled by the number of particles in low-j and high-j orbitals, in the different $\mathcal{N}$ shells. The configurations can be defined relative to a ^{132}Sn core as

$$\pi(g_{9/2})^{-p_1}(dg)^{p_2}(h_{11/2})^{p_3},$$
$$\nu(sd)^{-n_1}(h_{11/2})^{-n_2}(hf)^{n_3}(i_{13/2})^{n_4},$$

for which the short-hand notation $[(p_1)p_2p_3,n_1n_2(n_3n_4)]$ is employed. The pseudospin partners $d_{5/2}g_{7/2}\,(dg)$, $s_{1/2}d_{3/2}\,(sd)$, and $h_{9/2}f_{7/2}\,(hf)$ are not distinguished in the CNS formalism. Note that all particles are listed, and not just those considered to be active (unpaired). Note also that the labels do not refer to the pure j shells, but to the dominating amplitudes in the Nilsson orbitals, and in some cases, for an odd number of particles in a group, the signature is specified as the subscript $+(\alpha = +1/2)$ or $-(\alpha = -1/2)$. The $A = 130$ parameters introduced in Refs. [20,21] have been employed for the calculations on ^{134}Ce.

In the ^{134}Ce nucleus, the lowest proton configuration has eight protons in the $\pi g_{7/2}$ and $\pi d_{5/2}$ orbitals which interact and are strongly mixed. Higher angular momenta from proton configurations can be obtained by exciting one, two, or three protons from the $\pi g_{7/2}$ and $\pi d_{5/2}$ orbitals into the $\pi h_{11/2}$ one. The lowest observed bands are characterized by the configurations with the active neutron holes in the $\nu d_{3/2}$ and $\nu s_{1/2}$ orbitals, which interact and mix strongly. Higher angular momenta can be generated from neutron configurations with one, two, or three active holes in the $\nu h_{11/2}$ state instead. More excited states and very high angular momenta can then result from neutron excitations across the $N = 82$ shell gap into the $\nu f_{7/2}$, $\nu h_{9/2}$, and $\nu i_{13/2}$ orbitals and proton excitations from the $\pi g_{9/2}$ orbital across the $Z = 50$ shell gap.

Energies of the experimental bands observed in ^{134}Ce relative to a standard rotating liquid drop reference, E_{rld}(def) are presented in Fig. 8. As in the case of other triaxial bands observed in this mass region, the energy relative to a rotating liquid drop for medium- and high-spin bands displays a parabolic behavior. In contrast, the lowest excited bands have an upsloping behavior resulting from the increasing importance of pairing with decreasing spin, as recently discussed, for example, in Ref. [14]. The single-particle alignment for each band, extracted assuming a rotating reference with variable moment of inertia $\mathcal{I}_{\rm ref} = \mathcal{I}_0 + \omega^2\mathcal{I}_1$ with Harris parameters [31] $\mathcal{I}_0 = 17\ \hbar^2\,{\rm MeV}^{-1}$ and $\mathcal{I}_1 = 20\ \hbar^4\,{\rm MeV}^{-3}$, is provided in Fig. 9. The configuration assignments discussed below are proposed on the basis of achieving the best possible agreement between experimental and calculated band properties, such as excitation energies and spins, the configuration minima in the $E - E_{rld}$ plot, and the single-particle alignments.

A. The dipole bands

In ^{134}Ce, the dipole bands appear as nearly degenerate signature doublet sequences as evidenced in Fig. 8. The missing signature splitting signals instability in the tilt of the rotational axis with respect to the principal axes and the need to carry out tilted axis cranking (TAC) calculations. Nevertheless, as recently discussed in Ref. [16], the shape and energy are accounted for with good accuracy by the CNS calculations, and the interpretations advanced here are based on the results of the latter model.

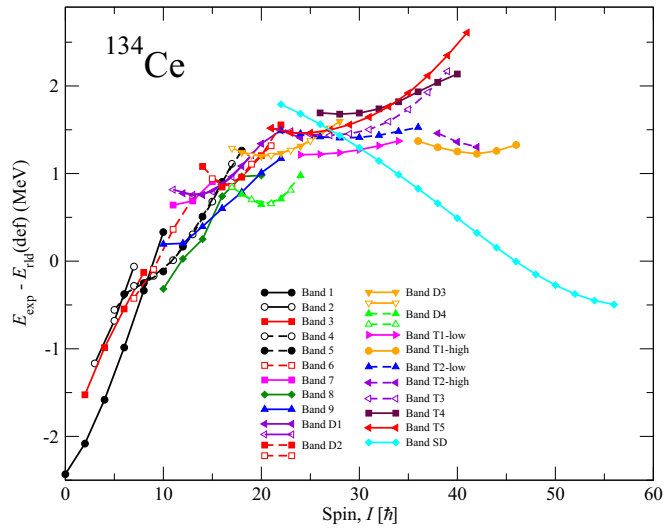

FIG. 8. Energies relative to a standard rotating liquid drop reference calculated for the experimental bands observed in ^{134}Ce. With an odd number of $h_{11/2}$ neutron holes, two signature degenerate bands are formed which are shown by the same color and symbols.

A comparison between experimental dipole bands and the proposed CNS configurations is presented in Fig. 10; the agreement between the data and calculations is within a few hundred keV. The calculations have been performed up to the highest spins for all possible configurations involving orbitals located around the Fermi surface. For such calculations, and in general when investigating configurations with degenerate signature doublets (such as those assigned to the dipole bands), it is natural to assume that states without neutrons excited above the $N = 82$ spherical shell closure can be assigned to nearly all bands, with the exception of band $D3$,

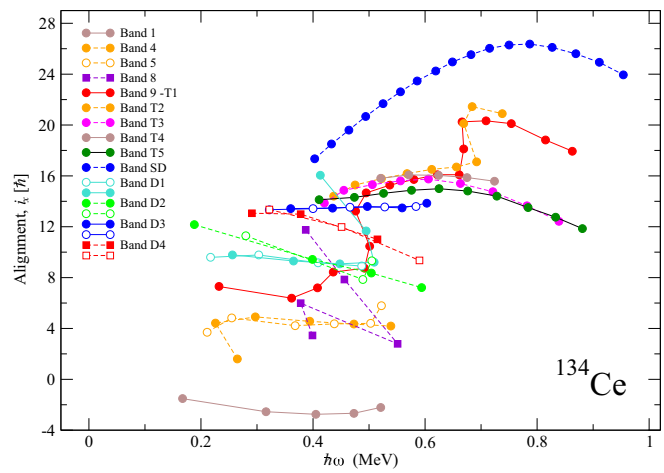

FIG. 9. Single-particle alignments for the bands in ^{134}Ce.

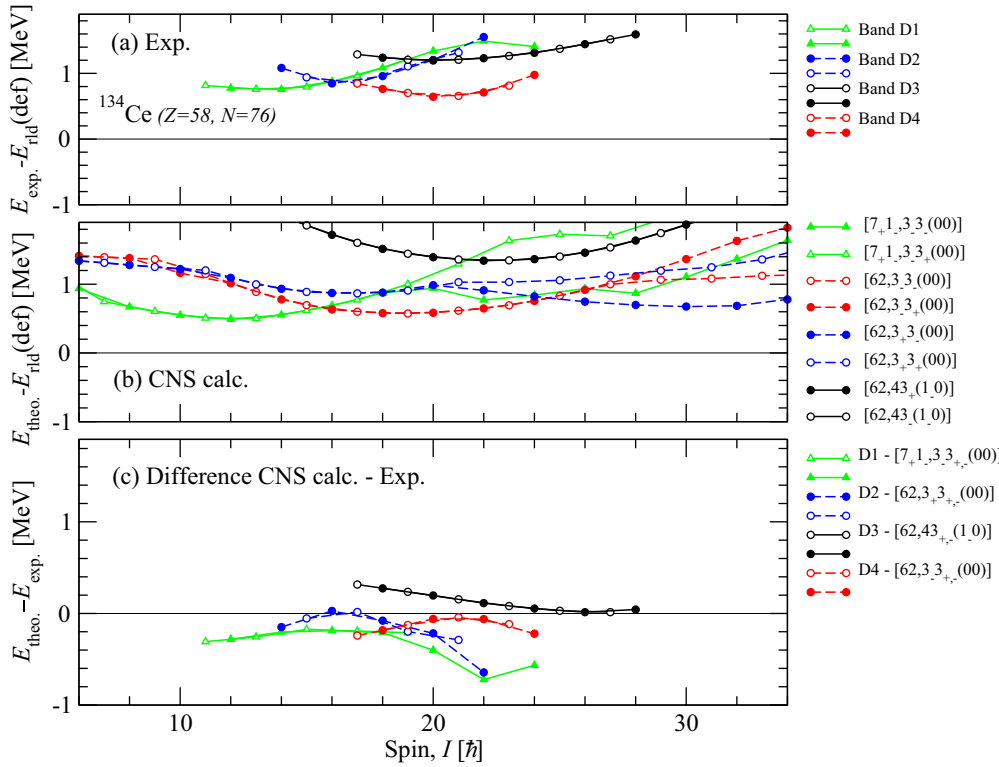

FIG. 10. The observed dipole bands of ^{134}Ce are shown relative to a rotating liquid drop reference in the upper panel, with the calculated configurations assigned to these bands given relative to the same reference in the middle panel. The lower panel provides the difference between calculations and experiment.

whose configuration has to involve one neutron excited to the $\nu(h_{9/2}f_{7/2})$ orbital, because of the high angular momenta involved (see Fig. 9).

The configuration assigned to band $D1$ is obviously different from the two possible negative-parity configurations $\pi h^2_{11/2} \otimes \nu h^{-1}_{11/2} d^{-1}_{3/2}$ and $\pi g^2_{7/2} \otimes \nu h^{-1}_{11/2} d^{-1}_{3/2}$ proposed in Ref. [5], since the present results clearly indicate this band to be of positive parity. The lowest positive-parity configuration with a minimum in the $E - E_{rld}$ plot around $I = 15$ (see Fig. 10) is $[7_+1_-,3_-3_\pm(00)]$, or $(dg)^1 \pi h^1_{11/2} \otimes \nu h^{-1}_{11/2}(sd)^{-1}$ in terms of spherical orbitals. Note that p_1 is omitted in the CNS shorthand notation unless it is nonzero. The calculated quadrupole deformation of this configuration decreases gradually from $\varepsilon_2 \sim 0.18$ to $\varepsilon_2 \sim 0.14$ at high spins, while the triaxiality parameter γ remains nearly constant, with $\gamma \approx +26^\circ$ up to $I = 22$. As one can see in Fig. 10, only the band with even spins involving the positive signature of the $\nu h_{11/2}$ orbital is observed at high spins. This behavior is well reproduced by the CNS calculations, which indicate a sudden change in the triaxial deformation of the even-spin partner from $\gamma \approx +25^\circ$ to $\gamma \approx -90^\circ$ occurring at $I = 18$, which induces the splitting between the two signature partners seen in Fig. 10, with the even-spin states favored energetically. The same shape change is also calculated for the odd-spin partner, but at spin $I = 23$, where the band is at a very high excitation energy and not observed experimentally. The upbend at $\hbar\omega \sim 0.45$ MeV in the alignment of band $D1$ (Fig. 9) is, therefore, induced by a shape change rather than by a quasiparticle alignment. This sudden change of shape or, alternatively, of the rotation axis of the triaxial nucleus from the short to the long axis, is quite unique and has been only rarely observed experimentally. A similar evolution of a dipole band in which only one signature partner extends to high spins was recently reported in ^{133}La [32]; however, in that case the rotation axis changed from a $3D$ direction to a principal axis. Another example of a switch of the rotation axis in a given configuration was recently observed in two high-spin bands of ^{138}Nd [13], wherein the triaxiality parameter γ changed from a positive to a negative value or, alternatively, the rotation axis changed from the short to the intermediate one.

The configuration assigned to band $D2$, $[62,3_+3_\pm(00)]$ or $\pi h^2_{11/2} \otimes \nu(sd)^{-1} h^{-1}_{11/2}$ in terms of spherical orbitals, is also different from the $\pi(g_{7/2}h_{11/2}) \otimes \nu h^{-2}_{11/2}$ one assigned to the same band in Ref. [5]. It is the next lowest excited four-quasiparticle configuration that can be obtained by a simple proton excitation relative to band $D1$, from the $\pi(dg)$ orbital to the $\pi h_{11/2}$ one. The deformation of this configuration and its evolution are similar to those of band $D1$, but in this case the shape change of the two signature partners is from $\gamma \approx +23^\circ$ to $\gamma \approx -30^\circ$ and occurs at similar spins of $I = 18$ and $I = 19$ for the even- and odd-spin partner, respectively. Thus, there is again a switch of the rotation axis from the short to the intermediate one, as in the case for the high-spin bands of ^{138}Nd [13], favoring the even-spin states in a manner similar to that seen in band $D1$. This also explains why one observes higher spins in this signature partner.

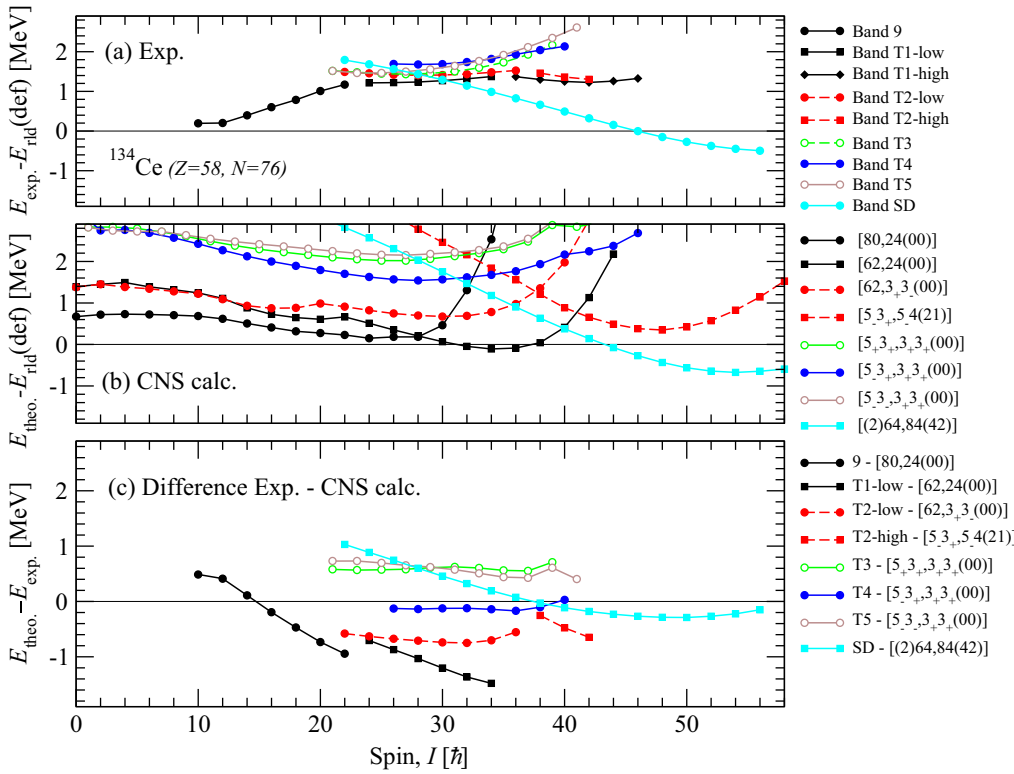

FIG. 11. The observed high-spin bands of ^{134}Ce are provided relative to a rotating liquid drop reference in the upper panel, with the calculated configurations assigned to these bands given relative to the same reference in the middle panel. The lower panel shows the difference between calculations and experiment.

The configurations assigned to the four-quasiparticle bands $D1$ and $D2$ in ^{134}Ce are closely related to those assigned to the three-quasiparticle bands 1 and 5 of ^{133}Ce [9], which are $[7_+1_-,43_\pm(00)]$ $(\pi(dg)^1 h^1_{11/2} \otimes \nu h^{-1}_{11/2})$ and $[62,43_\pm(00)]$ $(\pi h^2_{11/2} \otimes \nu h^{-1}_{11/2})$, respectively. The configurations of bands $D1$ and $D2$ are obtained simply by coupling one neutron hole in the $\nu(sd)$ orbital to the configurations of bands 1 and 5 of ^{133}Ce. A consistent description of the lowest dipole bands in the two nuclei is thus obtained.

The configuration proposed for the new band $D3$ is $[62,43_\pm(1\_0)]$, or $\pi h^2 \otimes \nu h^{-1}(hf)^1$ in terms of spherical orbitals. It represents a neutron excitation from the $\nu(sd)$ orbital to the $\nu(hf)$ one relative to bands $D1$ and $D2$. This accounts for both the higher excitation energy and the larger alignment of band $D3$ relative to bands $D1$ and $D2$ (see Fig. 9). The deformation of this configuration ($\varepsilon_2 \sim 0.21$) is larger than that of bands $D1$ and $D2$, and is rather stable as a function of spin. Such bands have been observed recently in the neighboring nucleus ^{133}Ce as well [19], and earlier in the isotone ^{136}Nd [33], where the two observed dipole bands 10 and 11 were satisfactorily reproduced using projected shell-model calculations by involving the $\nu(hf)$ orbital in the band configuration. Band $D3$, together with similar bands of ^{133}Ce and ^{136}Nd, provides clear evidence that dipole sequences may occur when orbitals from the $\nu(hf)$ subshell lying above the $N = 82$ spherical shell closure are involved, in addition to those from the nearly degenerate signature partners of the $\nu h_{11/2}$ orbital from the higher part of the $h_{11/2}$ subshell.

The configuration assigned to the new band $D4$ is $[62,3\_3_\pm(00)]$, or $\pi h^2_{11/2} \otimes \nu(sd)^{-1} h^{-1}_{11/2}$ in terms of spherical orbitals. The difference between this configuration and the $[62,3_+3_\pm(00)]$ one of band $D2$ is that one neutron is placed in the negative-signature of the $\nu(sd)$ orbital, which, in the spin range $I \approx 17$–24 (in which the band $D4$ is observed), has a driving force towards $\gamma \sim +23^\circ$, while the driving force of the neutron placed in the positive-signature orbital involved in the configuration of band $D2$ induces a shape with $\gamma \sim -30^\circ$. The calculated quadrupole deformation is practically constant at $\varepsilon_2 \approx 0.18$ in the observed spin range. As the moment of inertia for $\gamma \sim +23^\circ$ is smaller than that for $\gamma \sim -30^\circ$, the collective angular momentum is smaller as well and the alignment higher for the former, in agreement with experiment (see Fig. 9). One is, then, tempted to assign similar configurations to the bands $D2$ and $D4$, based on shapes with opposite triaxiality induced by the $\nu(sd)$ neutron placed in orbitals with opposite signature. The opposite triaxiality of the two bands leads to different collectivity and, consequently, to minima at different spins in the $E - E_{rld}$ plot (Fig. 10), larger for $\gamma \sim +23^\circ$.

B. The quadrupole high-spin bands

Comparisons between the experimental high-spin quadrupole bands and the assigned CNS configurations are given in Fig. 11. The configurations of bands $T2$, $T3$, and SD using TRS calculations have been discussed in Ref. [7]. It was concluded that the neutron configuration of the SD

band is $\nu(i_{13/2})^3 f_{7/2}^1$, with $\varepsilon_2 \sim 0.4$ and $\gamma \sim 0^\circ$, while the configurations of bands $T2$ and $T3$ are $\pi h^2 \otimes \nu h^{-3}(sd)^{-1}$ and $\pi h^2 \otimes \nu h^{-2}(sd)^{-2}$, respectively, with $\varepsilon_2 \sim 0.2$ and $\gamma \sim -30^\circ$.

The results of the present CNS calculations predict deformed shapes with $\varepsilon_2 \sim 0.15$–0.20 for the T bands and a triaxiality that changes with spin along the bands. These results are in disagreement with the previously proposed configurations assigned within the TRS framework.

The configuration originally assigned to band 9 is [80,24(00)], or $\nu h_{11/2}^{-2}$ in terms of spherical orbitals. This was based on g-factor measurements [34] which can be accounted for only by invoking a neutron configuration. These measurements indicate that band 8 is also based on a $\nu h_{11/2}^{-2}$ neutron configuration. The calculated deformation parameters of the yrast [80,24(00)] configuration change from ($\varepsilon_2 \sim 0.14, \gamma \sim -35^\circ$) to ($\varepsilon_2 \sim 0.12, \gamma \sim -49^\circ$) at $I = 12$. The upsloping behavior with decreasing spin of the difference between CNS calculations and experiment (see Fig. 11) is attributed to the fact that the calculations do not include pairing correlations which increase at lower spins. However, the average excitation energy of the band is correctly reproduced. Furthermore, when comparing with neighboring nuclei in which similar bands—i.e., bands built on the two lowest $I = 10^+$ states—have been observed (for example, in the isotone ^{136}Nd [35]), a deformation on the order of $\varepsilon_2 \sim 0.2$ is expected. This holds especially for a band which evolves regularly to high spins, as is the case for band 9. Therefore, the assignment of the calculated [80,24(00)] configuration with relatively small deformation to band 8, rather than to band 9, is justified, due to the irregular band pattern of band 8 which is characteristic of a shape being close to spherical. Thus, band 9 is based on a coexisting $\nu h_{11/2}^{-2}$ neutron configuration built on a minimum with larger deformation. For completeness, it should be mentioned that a different interpretation of bands 8 and 9 has recently been proposed in Ref. [36], based on results obtained using the multi-quasiparticle triaxial projected shell model. The bands built on the two lowest $I = 10^+$ states are interpreted as low-K $\nu h_{11/2}^{-2}$ configurations built on shapes with low deformation and nearly maximal triaxiality ($\varepsilon_2 = 0.150, \gamma = 34^\circ$).

Band $T1$ is the continuation at higher spins of band 9 and consists of two parts with different behavior: the part in the range $I = 24$–34 (labeled $T1$-low in Fig. 11) has a nearly flat pattern as a function of spin, while that in the range $I = 36$–46 (labeled $T1$-high in Fig. 11) displays a downsloping trend with increasing spin. The lowest, even-spin positive-parity configuration [62,24(00)], or $\pi h_{11/2}^2 \otimes \nu h_{11/2}^2$ in terms of spherical orbitals, is assigned to $T1$-low. Its calculated quadrupole deformation changes from $\varepsilon_2 \sim 0.16$ at $I = 24$ to $\varepsilon_2 \sim 0.12$ at $I = 34$, while the triaxiality parameter is nearly constant at $\gamma \sim -38^\circ$. The excitation energy of this configuration is calculated too low with respect to experiment and displays the upsloping behavior with decreasing spins characteristic of calculations without pairing correlations. To account for the downsloping behavior of band $T1$ at the highest spins, one has to involve neutron excitations into the $\nu\,(h_{9/2}, f_{7/2}$ and/or $i_{13/2})$ states above the $N = 82$ spherical shell closure. Unfortunately, it was not possible to find a reasonable agreement between the lowest calculated CNS configurations and data for the high-spin part of band $T1$ and the observations remain a challenge to explain.

The $E - E_{rld}$ plot of band $T2$ is similar to that of band $T1$, showing a nearly flat behavior in the spin range $I = 22$–36 (band $T2$-low in Fig. 11) and a downsloping trend in the spin range $I = 38$–42 (band $T2$-high in Fig. 11). As a result, the next lowest configuration with nearly flat behavior in the $I = 22$–36 spin range, which is [62,3$_+$3$_-$(00)], is assigned to band $T2$-low. This configuration involves a single neutron excitation from the $\nu(sd)$ orbital to the $h_{11/2}$ one relative to the lower part of band $T1$ and also has a deformation similar to that of the lower part of the latter band. Likewise, the high-spin part of band $T2$ has a behavior similar to the high-spin part of band $T1$. Therefore, the [5$_-$3$_+$,5$_-$4(21)] configuration is assigned to this part. The calculated deformation ($\varepsilon_2 \sim 0.26, \gamma \sim +20^\circ$) is definitely higher than that of the lower part of band $T2$, which is itself higher than that of the high-spin part of band $T1$.

As can be seen in Fig. 9, upbends are observed in bands $T1$ and $T2$ at $\hbar\omega \approx 0.68$ MeV, which correspond to the change of slope at spin $I = 36$ in Figs. 8 and 11. The alignment gains in bands $T1$ and $T2$ are induced by the occupation of the $\nu(hf)$ and $\nu i_{13/2}$ intruder orbitals, which have a strong driving force towards higher deformation. A similar behavior has been observed in the negative-parity yrast sequence of ^{135}Pr, where a crossing was observed at $\hbar\omega \approx 0.63$ MeV, with a similar spin gain of $\sim 4\,\hbar$ [8]. This speaks in favor of the [5$_-$3$_+$,44(1$_+$1)] and [5$_-$3$_+$,5$_-$4(21)] configurations for the high-spin parts of bands $T1$ and $T2$, respectively, obtained through the excitation of two and three neutrons into the $\nu(hf)$ and $\nu i_{13/2}$ intruder orbitals. Such a configuration change also leads to an increased deformation ($\varepsilon_2 \sim 0.25, \gamma \sim +25^\circ$) and to a jump into the highly-deformed HD minimum, extensively studied in the Nd nuclei.

Bands $T3$, $T4$, and $T5$ exhibit a behavior similar to the low-spin parts of bands $T1$ and $T2$ (see Figs. 8 and 9). Therefore, it is natural to assign a similar configuration to these bands; i.e., those without neutrons excited into the $\nu(hf)$ and $\nu i_{13/2}$ orbitals. Thus, bands $T3$, $T4$, and $T5$ are assigned [5$_+$3$_+$,3$_+$3$_+$(00)], [5$_-$3$_+$,3$_+$3$_+$(00)], and [5$_-$3$_-$,3$_+$3$_+$(00)] configurations, respectively.

The configuration assigned to the SD band in the present work is different from that proposed in Ref. [7] using TRS calculations. It is based on the behavior of the band (see Figs. 8 and 9), which cannot be accounted for by the $\nu(hf)^1 i^2$ configuration that has its minimum in the $E - E_{rld}$ plot much lower than the experimental one located at $I > 50$ (see Fig. 8). The most probable configuration of the SD band is [(2)64,84(42)] or $\pi(g^{-2})(dg)^6 h_{11/2}^4 \otimes \nu(hf)^4 i^2$ in terms of spherical orbitals, with six neutrons excited to the intruder orbitals $\nu(hf)$ and $\nu i_{13/2}$, two proton holes in the $\pi g_{9/2}$ orbital, and a prolate deformation of ($\beta_2 \sim 0.4, \gamma \sim 0^\circ$). The two additional neutrons in the $\nu i_{13/2}$ orbital relative to the configurations assigned to the high-spin parts of bands $T1$ and $T2$ account for the aligned spin of the SD band, which is higher by $\sim 5\,\hbar$ than that of these two bands (see Fig. 9). The configuration assigned to this SD band has one additional neutron placed in the $\nu i_{13/2}$ intruder orbital, relative to the

[(2)64,83($3_{\pm}$2)] configurations assigned to the bands SD1 and SD2 of ^{133}Ce, which have behavior similar to that of the ^{134}Ce SD band. With these configuration assignments, one achieves a consistent description for the SD excitations in the ^{133}Ce and ^{134}Ce nuclei.

V. SUMMARY

High-spin states in ^{134}Ce have been investigated using the ^{116}Cd(^{22}Ne ,4n) reaction and the Gammasphere array. The primary aim of this investigation has been to further elucidate the role of triaxiality in nuclei in this mass region, as evidenced by the observation of chiral and wobbling bands, both unique signatures of triaxiality, in nearby nuclei. An extended level scheme has been developed with many important differences with respect to previously published results. New bands of quadrupole and dipole transitions were identified up to high spins. The observed bands have been discussed within the CNS model and a consistent interpretation of the well-developed bands has been achieved. The global understanding of the observed bands renders strong support to the existence of triaxial nuclear shapes at medium and high spin in this mass region and sheds new light on the excitations in the SD minimum in the Ce nuclei.

ACKNOWLEDGMENTS

C.M.P. expresses his gratitude to Prof. I. Ragnarsson for providing the CNS codes, for the training on how to use them, and for enlightening comments on the theoretical interpretation of the results. This work has been supported in part by the US National Science Foundation (Grants No. PHY07-58100, No. PHY-0822648, No. PHY-1068192, and No. PHY-1419765), the US Department of Energy, Office of Nuclear Physics, under Grant No. DE-FG02-94ER40834 (UM), and Contract No. DE-AC02-06CH11357 (ANL). This research used resources of ANL's ATLAS facility, which is a DOE Office of Science User Facility.

[1] D. Husar *et al.*, Nucl. Phys. A **292**, 267 (1977).
[2] M. B. Goldberg *et al.*, Phys. Lett. B **97**, 351 (1980).
[3] M. Müller-Veggian *et al.*, Nucl. Phys. A **417**, 189 (1984).
[4] E. Dafni *et al.*, Phys. Lett. B **181**, 21 (1986).
[5] S. Lakshmi, H. C. Jain, P. K. Joshi, A. K. Jain, and S. S. Malik, Phys. Rev. C **69**, 014319 (2004).
[6] A. Gade *et al.*, Nucl. Phys. A **673**, 45 (2000).
[7] N. J. O'Brien *et al.*, Phys. Rev. C **59**, 1334 (1999).
[8] E. S. Paul, C. Fox, A. J. Boston, H. J. Chantler, C. J. Chiara, R. M. Clark, M. Cromaz, M. Descovich, P. Fallon, D. B. Fossan, A. A. Hecht, T. Koike, I. Y. Lee, A. O. Macchiavelli, P. J. Nolan, K. Starosta, R. Wadsworth, and I. Ragnarsson, Phys. Rev. C **84**, 047302 (2011).
[9] A. D. Ayangeakaa *et al.*, Phys. Rev. Lett. **110**, 172504 (2013).
[10] J. T. Matta, U. Garg, W. Li, S. Frauendorf, A. D. Ayangeakaa, D. Patel, K. W. Schlax, R. Palit, S. Saha, J. Sethi, T. Trivedi, S. S. Ghugre, R. Raut, A. K. Sinha, R. V. F. Janssens, S. Zhu, M. P. Carpenter, T. Lauritsen, D. Seweryniak, C. J. Chiara, F. G. Kondev, D. J. Hartley, C. M. Petrache, S. Mukhopadhyay, D. V. Lakshmi, M. K. Raju, P. V. Madhusudhana Rao, S. K. Tandel, S. Ray, and F. Donau, Phys. Rev. Lett. **114**, 082501 (2015).
[11] A. V. Afanasjev and I. Ragnarsson, Nucl. Phys. A **608**, 176 (1996).
[12] C. M. Petrache, S. Frauendorf, M. Matsuzaki, R. Leguillon, T. Zerrouki, S. Lunardi, D. Bazzacco, C. A. Ur, E. Farnea, C. Rossi Alvarez, R. Venturelli, and G. de Angelis, Phys. Rev. C **86**, 044321 (2012).
[13] C. M. Petrache, I. Ragnarsson, H.-L. Ma, R. Leguillon, T. Konstantinopoulos, T. Zerrouki, D. Bazzacco, and S. Lunardi, Phys. Rev. C **88**, 051303(R) (2013).
[14] C. M. Petrache, I. Ragnarsson, H.-L. Ma, R. Leguillon, T. Zerrouki, D. Bazzacco, and S. Lunardi, Phys. Rev. C **91**, 024302 (2015).
[15] R. Leguillon and C. M. Petrache *et al.*, Phys. Rev. C **88**, 014323 (2013).
[16] T. Zerrouki and C. M. Petrache *et al.*, Eur. Phys. J. A **51**, 50 (2015).
[17] C. M. Petrache *et al.*, Phys. Scr. **90**, 114016 (2015).
[18] K. Hauschild, R. Wadsworth, R. M. Clark, I. M. Hibbert, P. Fallon, A. O. Macchiavelli, D. B. Fossan, H. Schnare, I. Thorslund, P. J. Nolan, A. T. Semple, and L. Walker, Phys. Rev. C **54**, 613 (1996).
[19] A. D. Ayangeakaa, U. Garg, C. M. Petrache, S. Guo, P. W. Zhao, J. T. Matta, B. K. Nayak, D. Patel, R. V. F. Janssens, M. P. Carpenter, C. J. Chiara, F. G. Kondev, T. Lauritsen, D. Seweryniak, S. Zhu, S. S. Ghugre, and R. Palit, Phys. Rev. C **93**, 054317 (2016).
[20] A. V. Afanasjev, D. B. Fossan, G. J. Lane, and I. Ragnarsson, Phys. Rep. **322**, 1 (1999).
[21] T. Bengtsson and I. Ragnarsson, Nucl. Phys. A **436**, 14 (1985).
[22] B. G. Carlsson and I. Ragnarsson, Phys. Rev. C **74**, 011302 (2006).
[23] A. V. Afanasjev and I. Ragnarsson, Nucl. Phys. A **591**, 387 (1995).
[24] I-Yang Lee, Nucl. Phys. A **520**, c641 (1990).
[25] D. C. Radford, Nucl. Instrum. Methods Phys. Res. A **361**, 297 (1995).
[26] D. C. Radford, Nucl. Instrum. Methods Phys. Res. A **361**, 306 (1995).
[27] V. Iacob and G. Duchene, Nucl. Instrum. Methods Phys. Res. A **399**, 57 (1997).
[28] A. Krämer-Flecken, T. Morek, R. M. Lieder, W. Gast, G. Hebbinghaus, H. M. Jäger, and W. Urban, Nucl. Instrum. Meth. Phys. Res. A **275**, 333 (1989).
[29] C. J. Chiara, M. Devlin, E. Ideguchi, D. R. LaFosse, F. Lerma, W. Reviol, S. K. Ryu, D. G. Sarantites, O. L. Pechenaya, C. Baktash, A. Galindo-Uribarri, M. P. Carpenter, R. V. F. Janssens, T. Lauritsen, C. J. Lister, P. Reiter, D. Seweryniak, P. Fallon, A. Görgen, A. O. Macchiavelli, D. Rudolph, G. Stoitcheva, and W. E. Ormand, Phys. Rev. C **75**, 054305 (2007).
[30] E. Dafni, F. D. Davidovsky, A. Gelberg, M. Haas, E. Naim, and G. Schatz, Hyperfine Interact. **15**, 101 (1983).
[31] S. M. Harris, Phys. Rev. **138**, B509 (1965).

[32] C. M. Petrache *et al.* (unpublished).
[33] C. M. Petrache, Y. Sun, D. Bazzacco, S. Lunardi, C. RossiAlvarez, R. Venturelli, D. De Acuna, G. Maron, M. N. Rao, Z. Podolyak, and J. R. B. Oliveira, Phys. Rev. C **53**, R2581 (1996).
[34] A. Zemel, C. Broude, E. Dafni, A. Gelberg, J. Gerber, G. J. Kumbartzki, and K. H. Speidel, Nucl. Phys. A **383**, 165 (1982).
[35] C. M. Petrache *et al.*, Phys. Lett. B **373**, 275 (1996).
[36] J. A. Sheikh *et al.*, Nucl. Phys. A **824**, 58 (2009).